

On very short and intense laser-plasma interactions

Gaetano Fiore

Dip. di Matematica e Applicazioni, Università “Federico II”
V. Claudio 21, 80125 Napoli, Italy;
I.N.F.N., Sez. di Napoli, Complesso MSA, V. Cintia, 80126 Napoli, Italy

Abstract

We briefly report on some results regarding the impact of very short and intense laser pulses on a cold, low-density plasma initially at rest, and the consequent acceleration of plasma electrons to relativistic energies. Locally and for short times the pulse can be described by a transverse plane electromagnetic travelling-wave and the motion of the electrons by a purely Magneto-Fluido-Dynamical (MFD) model with a very simple dependence on the transverse electromagnetic potential, while the ions can be regarded as at rest; the Lorentz-Maxwell and continuity equations are reduced to the Hamilton equations of a Hamiltonian system with 1 degree of freedom, in the case of a plasma with constant initial density, or a collection of such systems otherwise. We can thus describe both the well-known *wakefield* behind the pulse and the recently predicted *slingshot effect*, i.e. the backward expulsion of high energy electrons just after the laser pulse has hit the surface of the plasma.

1 Introduction and preliminaries

Today the acceleration of charged particles to relativistic energies has a host of important applications, in particular in:

1. nuclear medicine, cancer therapy (PET, electron/proton therapy,...);
2. research in structural biology;
3. research in materials science;

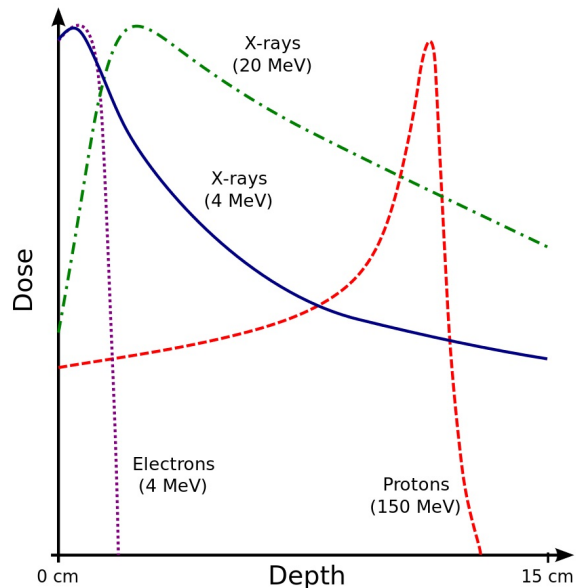


Figure 1: Left: rates of absorption of the beam energy by a living tissue (doses) vs. the depth of penetration of the beam. Right: water wave and surfing.

4. food sterilization;
5. research in nuclear fusion (inertial fusion);
6. transmutation of nuclear wastes;
7. research in high-energy particle physics.

Let us just mention the main advantage of attacking a cancer by particle rather than by radiation therapy. As the dose of X- or gamma-rays absorbed by human tissue depends weakly on the depth (see fig. 1 left), if the cancer is well localized the beam damages not only the sick tissue but also the healthy one. On the contrary, electron therapy is particularly suited for skin and other superficial cancers, because the dose of electrons (beta rays) practically vanishes beyond 1-2 cm, whereas proton and more generally ion therapy is particularly suited for deeper cancers, because the dose of ions has its maximum (the *Bragg peak*) at a depth tunable up to 15-20 cm. In fact, in either case the collision cross-section with water molecules is strongly energy dependent, and the depth at which most energy is deposited in human tissue can be fine-tuned. Today 58 proton and 8 carbon ion therapy centers exist (resp. 21, 3 in Europe); more are planned or under construction. All have big

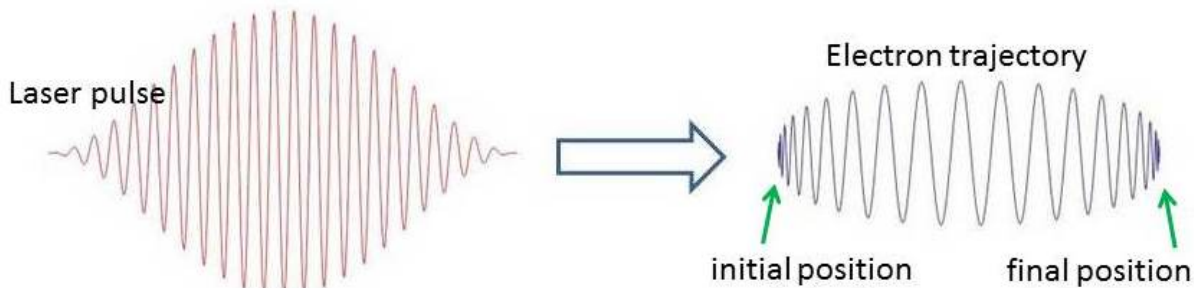


Figure 2: Sample laser pulse and consequent motion in vacuum of an electron initially at rest.

size, high cost, high complexity; for instance, the CNAO hadron therapy center in Pavia uses a 25m diameter synchrotron which has costed about 100 MEuro. In fact, past and present-day acceleration techniques (cyclotrons, synchrotrons,...) rely on the interaction of radio-frequency electromagnetic (EM) waves with ‘few’ charged particles (those one wishes to accelerate) over long distances. The main reason of these structural limits is that electric fields cannot exceed the threshold of material breakdown (due to discharge sparks between electrodes) of $10 \div 100\text{MeV/m}$, therefore accelerating an electron or a proton to 1 GeV even by the most powerful machines requires a distance of 50-100 m. The search for alternative acceleration mechanisms is therefore of great importance.

In vacuum, a coherent EM wave (laser pulse) reaching a charged particle at rest induces a motion composed of a transverse oscillation and a drift in the longitudinal direction \hat{z} of propagation of the pulse, as depicted in fig. 2. This drift is caused by the ponderomotive force $F_p := \langle -e(\frac{\mathbf{v}}{c} \times \mathbf{B})^z \rangle$ generated by the pulse; here $\langle \rangle$ is the average over a period of the laser carrier wave, \mathbf{E} , \mathbf{B} are the electric and magnetic fields, \mathbf{v} is the electron velocity, c is the speed of light, \hat{z} is the direction of propagation of the laser pulse; F_p is positive (negative) while the modulating amplitude ϵ_s of the pulse respectively grows (decreases). During very intense laser pulses the particle becomes relativistic, but under broad conditions its initial and final energies are practically equal, i.e. no net energy gain is possible; this is the so-called ‘Lawson-Woodward theorem’ [3, 4, 5, 6].

One can try to evade the theorem by laser-matter, more precisely laser-plasma interactions (by the way, very intense laser pulse locally ionize matter and convert it into a plasma). An intense laser beam (alternatively, a beam of high energy protons/electrons) travelling in a plasma causes large longitudinal charge density variations (lighter electrons are displaced with respect to heavier ions) and thus a huge longitudinal electric field \mathbf{E} , due to the huge numbers of electrons and ions present. These variations arrange in a wake of waves (*plasma*

waves) traveling with phase velocity close to c : electrons are several times boosted forth and back, squeezed and unsqueezed, but are again left behind the laser beam with low speed. This is similar to the fate of most water molecules in water waves. However, if some foam at the crest of a water wave is a bit faster than the surrounding water, then it is accelerated ‘surfing’ down the water wave slope (see fig. 1 right). Similarly, if some electrons are injected faster than their neighbours, they can be accelerated ‘surfing’ down the plasma wake waves: this is the so-called *Wake-Field Acceleration* (WFA) mechanism conceived by Tajima and Dawson [7]. Such electrons are finally expelled out of the plasma sample behind the beam, in the same direction. The WFA is especially effective in the *bubble regime*, where the ‘troughs’ of the wake correspond to ‘ion bubbles’ deprived of electrons: it yields nearly monochromatic and collimated electron bunches of high energy. However, the onset of the bubble regime is not under full control yet. Records established using laser pulses of wavelength $\lambda \sim 1\mu\text{m}$, length $l \sim 10\mu\text{m}$, energy \mathcal{E} , hitting helium jets of electron density $n_0 = 10^{17} \div \times 10^{19}\text{cm}^{-3}$ are:

- 200 MeV electrons were obtained in 2004 using $\mathcal{E} \sim 1\text{J}$ laser pulses [8, 9, 10].
- $2 \div 5$ GeV electrons were obtained in 2013-14 using $\mathcal{E} \lesssim 150\text{J}$ laser pulses (by a PetaWatt laser) [11].

We have recently suggested [1, 2] the existence of one more acceleration mechanism: the impact of a very short and intense laser pulse in the form of a pancake normally onto the surface of a low-density plasma may induce also the acceleration and expulsion of electrons backwards (*slingshot effect*), see fig. 3. A bunch of plasma electrons - in a thin layer just beyond the vacuum-plasma interface - first are displaced forward with respect to the ions by the ponderomotive force generated by the pulse, then are pulled back by the electric force $-eE^z$ due to this charge displacement. Tuning the electron density \tilde{n}_0 in the range where the plasma oscillation period T_H ¹ is about twice the pulse duration τ , we can make these electrons invert their motion when they are reached by the maximum of ϵ_s , so that the negative part of F_p adds to $-eE^z$ in accelerating them backwards; thus the total work $W = \int_0^\tau dt F_p \langle v^z \rangle$ done by the ponderomotive force is maximal. The radius R of the laser spot should be “small”, for the pulse intensity - as well as the final energy of the expelled electrons escaping to $z \rightarrow -\infty$ - to be “large”, but not so small that lateral electrons obstruct them the way out backwards. If $\tau \ll T_H$, then while the pulse is passing the electric force due to charge separation can be neglected, and the motion of the electron is close to the one in vacuum (fig. 2); the backward acceleration takes place afterwards and is due only to $-eE^z$,

¹ T_H grows with the oscillation amplitude ζ , but goes to the nonrelativistic period $T_H^{\text{nr}} = \sqrt{\pi m/n_0 e^2}$ as $\zeta \rightarrow 0$

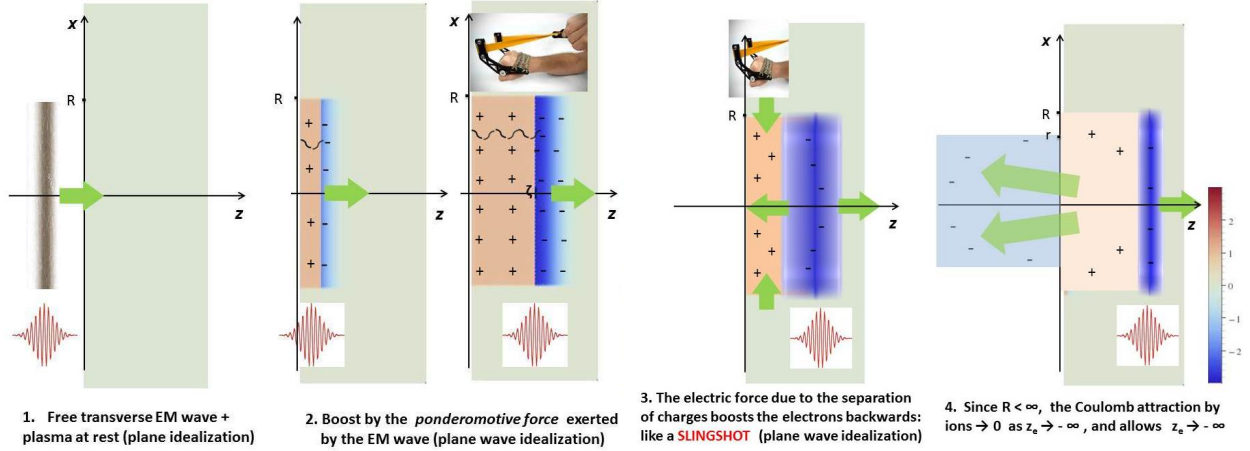


Figure 3: Schematic stages of the slingshot effect

hence the final energy is smaller. Whereas if $\tau \gg T_H$ - which was the standard situation in laboratories until a couple of decades ago - then $F_p v^z$ oscillates many times about 0, $W \simeq 0$, and the slingshot effect is washed out.

Very short τ 's and huge nonlinearities make approximation schemes based on Fourier analysis and related methods inconvenient. On the contrary, in [2, 12] it is shown that in the relevant space-time region a MFD description of the impact is self-consistent, simple and predictive, without need of a recourse to kinetic theory (i.e to a statistical description in phase space) taking collisions into account, e.g. by BGK [13] equations or effective linear inheritance relations [14]. The set-up is as follows. We regard the plasma as collisionless, with the ions at rest and a fully relativistic fluid of electrons; the system “plasma + electromagnetic field” fulfills the Lorentz-Maxwell and the continuity Partial Differential Equations (PDE). For brevity, below we refer to the electrons’ fluid element initially located at $\mathbf{X} \equiv (X, Y, Z)$ as to the “ \mathbf{X} electrons”, and to the fluid elements with arbitrary X, Y and specified Z as the “ Z electrons”. We denote: as $\mathbf{x}_e(t, \mathbf{X})$ the position at time t of the \mathbf{X} electrons, and for each fixed t as $\mathbf{X}_e(t, \mathbf{x})$ the inverse of $\mathbf{x}_e(t, \mathbf{X})$ [$\mathbf{x} \equiv (x, y, z)$]; as m and as $n, \mathbf{v}, \mathbf{p}$ the electrons’ mass and Eulerian density, velocity, momentum. $\boldsymbol{\beta} := \mathbf{v}/c$, $\mathbf{u} := \mathbf{p}/mc = \boldsymbol{\beta}/\sqrt{1-\boldsymbol{\beta}^2}$, $\gamma := 1/\sqrt{1-\boldsymbol{\beta}^2} = \sqrt{1+\mathbf{u}^2}$ are dimensionless. Lagrangian fields carry a $\tilde{}$ and are related to Eulerian ones by the relation $\tilde{f}(t, \mathbf{X}) = f[t, \mathbf{x}_e(t, \mathbf{X})]$. We assume that the plasma is initially neutral, unmagnetized and at rest with electron (and proton) density $\tilde{n}_0(Z)$ depending only on Z and equal to zero in the region $Z < 0$. We schematize the laser pulse as a free transverse EM plane travelling-wave multiplied by a cylindrically symmetric

“cutoff” function, e.g.

$$\mathbf{E}^\perp(t, \mathbf{x}) = \boldsymbol{\epsilon}^\perp(ct - z) \theta(R - \rho), \quad \mathbf{B}^\perp = \hat{\mathbf{z}} \times \mathbf{E}^\perp \quad (1)$$

where $\rho := \sqrt{x^2 + y^2} \leq R$, θ is the Heaviside step function, and the ‘pump’ $\boldsymbol{\epsilon}^\perp(\xi)$ vanishes outside some finite interval $0 < \xi < l$. Then, to simplify the problem:

1. We study the $R = \infty$ (i.e. *plane-symmetric*) version first, carefully choosing unknowns and independent variables (sect. 2.1). For small $\tilde{n}_0(Z)$ and short times we can reduce the PDE’s to a collection of decoupled *systems of two 1st order nonlinear ODE in Hamiltonian form*, which we solve numerically.
2. We determine (sect. 2.2): $R < \infty$ and a suitable positive $r \leq R$ so that the plane version gives small errors at least for \mathbf{X} electrons with $Z \gtrsim 0$ and $\sqrt{X^2 + Y^2} \leq r$ until their expulsions; sample final energies, spectra of the expelled electrons. For definiteness, we consider $\tilde{n}_0(Z)$ of the kind of fig. 4.

2 Model and predictions

2.1 Plane wave idealization

Here is our plane wave Ansatz: A^μ (the EM potential), $\mathbf{u}, n - \tilde{n}_0(z)$ depend only on z, t and vanish if $ct \leq z$; $\Delta \mathbf{x}_e := \mathbf{x}_e - \mathbf{X}$ depends only on Z, t and vanishes if $ct \leq Z$. Then: $\mathbf{B} = \mathbf{B}^\perp = \hat{\mathbf{z}} \wedge \partial_z \mathbf{A}^\perp$, $c\mathbf{E}^\perp = -\partial_t \mathbf{A}^\perp$; the transverse component of the Lorentz equation $d\mathbf{p}/dt = -e(\mathbf{E} + \frac{\mathbf{v}}{c} \wedge \mathbf{B})$ and the initial condition $\mathbf{p} \equiv 0$ imply $\mathbf{u}^\perp = e\mathbf{A}^\perp/mc^2$; by the continuity equation the Eulerian electron density n_e and the initial one \tilde{n}_0 are related through $n_e(t, z) = \tilde{n}_0[Z_e(t, z)] \partial Z_e(t, z)/\partial z$; by the Maxwell equations E^z is determined by the longitudinal motion and \tilde{n}_0 through

$$E^z(t, z) = 4\pi e \left\{ \tilde{N}(z) - \tilde{N}[Z_e(t, z)] \right\}, \quad \tilde{N}(Z) := \int_0^Z d\eta \tilde{n}_0(\eta); \quad (2)$$

the positive (resp. negative) term at the right-hand side is due to the ions (electrons). For sufficiently small densities and short times the laser pulse is not significantly affected by the interaction with the plasma (the validity of this approximation is checked a posteriori [2]), and we can identify $\mathbf{A}^\perp(t, z) = \boldsymbol{\alpha}(\xi)$, $\mathbf{u}^\perp(t, z) = e\boldsymbol{\alpha}(\xi)/mc^2 =: \hat{\mathbf{u}}^\perp(\xi)$ where $\xi := ct - z$, and $\boldsymbol{\alpha}(\xi) := -\int_0^\xi ds \boldsymbol{\epsilon}^\perp(s)$ is the transverse vector potential of the ‘pump’ free laser pulse. The remaining unknowns are $u^z(t, z)$ and $z_e(t, Z)$. In the equations of motion of the Z -electrons

(Lagrangian description) $z_e(t, Z)$ appears everywhere in place of z , e.g. the force associated to (2) is $\tilde{F}_e^z(t, Z) := 4\pi e^2 \left\{ \tilde{N}(Z) - \tilde{N}[z_e(t, Z)] \right\}$. This is conservative, since it depends on t only through $z_e(t, Z)$. As no particle can reach the speed of light, the map $t \mapsto \xi = \tilde{\xi}(t, Z) := ct - z_e(t, Z)$ is strictly increasing, and we can use (ξ, Z) *instead of* (t, Z) as independent variables, so that the argument ξ of $\hat{\mathbf{u}}^\perp$ is; we shall denote the dependence of a field on (ξ, Z) by a caret. It is also convenient to use the ‘electron s -factor’ $\hat{s} := \hat{\gamma} - \hat{u}^z$ instead of \hat{u}^z as an unknown, because $\hat{\gamma}, \hat{\mathbf{u}}, \hat{\boldsymbol{\beta}}$ are *rational* functions (no square roots!) of $\hat{\mathbf{u}}^\perp, \hat{s}$,

$$\hat{\gamma} = \frac{1 + \hat{\mathbf{u}}^{\perp 2} + \hat{s}^2}{2\hat{s}}, \quad \hat{u}^z = \frac{1 + \hat{\mathbf{u}}^{\perp 2} - \hat{s}^2}{2\hat{s}}, \quad \hat{\boldsymbol{\beta}} = \frac{\hat{\mathbf{u}}}{\hat{\gamma}} \quad (3)$$

(these relations hold also with the caret replaced by a tilde or nothing), and - as we will show - \hat{s} is *insensitive* to rapid oscillations of $\boldsymbol{\alpha}$. The definitions $\tilde{\boldsymbol{\beta}} := \tilde{\mathbf{v}}/c = \partial \mathbf{x}_e / c \partial t$ and $\tilde{s} := \tilde{\gamma} - \tilde{u}^z = \sqrt{1 + \tilde{\mathbf{u}}^2} - \tilde{u}^z$, together with the Lorentz equation (in Lagrangian formulation) $\partial \tilde{\mathbf{u}} / \partial t = -e(\tilde{\mathbf{E}} + \tilde{\boldsymbol{\beta}} \wedge \tilde{\mathbf{B}}) / mc$, lead to

$$\frac{1}{c} \frac{\partial (\mathbf{x}_e - \mathbf{X})}{\partial t} = \tilde{\boldsymbol{\beta}} \stackrel{(3)}{=} \frac{\tilde{\mathbf{u}}}{\tilde{\gamma}}, \quad \tilde{\gamma} \frac{\partial \tilde{s}}{\partial t} = -\frac{\tilde{F}_e^z}{mc} \tilde{s} + \tilde{g} = \frac{4\pi e^2}{mc} \left\{ \tilde{N}[z_e(t, Z)] - \tilde{N}(Z) \right\} \tilde{s} + \tilde{g},$$

where $g := (\partial_t + c\partial_z) \mathbf{u}^{\perp 2}$. Since $g \equiv 0$ in our approximation $\mathbf{u}^\perp(t, z) = \hat{\mathbf{u}}^\perp(ct - z)$ and $c\hat{s}\partial/\partial\xi = \tilde{\gamma}\partial/\partial t$, then, switching to the independent variables ξ, Z we find

$$(\hat{\mathbf{x}}_e^\perp - \mathbf{X}^\perp)' = \hat{\mathbf{u}}^\perp / \hat{s}, \quad \hat{\mathbf{x}}_e^\perp(0, Z) - \mathbf{X}^\perp = 0, \quad (4)$$

$$\hat{\Delta}' = \frac{1+v}{2\hat{s}^2} - \frac{1}{2}, \quad \hat{s}' = \frac{4\pi e^2}{mc^2} \left\{ \tilde{N}[\hat{\Delta} + Z] - \tilde{N}(Z) \right\} \quad (5)$$

$$\hat{\Delta}(0, Z) = 0, \quad \hat{s}(0, Z) = 1. \quad (6)$$

Here $\hat{\Delta}(\xi, Z) := \hat{z}_e(t, Z) - Z$ is the electrons’ longitudinal displacement with respect to the initial equilibrium position Z , $f' := \partial f / \partial \xi$, $v(\xi) := \hat{\mathbf{u}}^{\perp 2}(\xi)$.

The PDE to be solved are reduced to the collection (5-6) of systems (parametrized by Z) of first order ODE’s in the unknowns $\hat{\Delta}(\xi, Z)$, $\hat{s}(\xi, Z)$. In fact we now show how determine all unknowns once (5-6) is solved. Let

$$\begin{aligned} \hat{\mathbf{Y}}^\perp(\xi, Z) &:= \int_0^\xi d\xi' \frac{\hat{\mathbf{u}}^\perp(\xi')}{\hat{s}(\xi', Z)}, & \hat{Y}^z(\xi, Z) &:= \int_0^\xi d\xi' \frac{\hat{u}^z(\xi', Z)}{\hat{s}(\xi', Z)}, \\ \hat{\Xi}(\xi, Z) &:= \int_0^\xi d\xi' \frac{\hat{\gamma}(\xi', Z)}{\hat{s}(\xi', Z)}, & \hat{c}t(\xi, Z) &:= \xi + \hat{z}_e(\xi, Z); \end{aligned} \quad (7)$$

by (3), (5) it is also $\hat{Y}^z \equiv \hat{\Delta}$, $\hat{\Xi}(\xi, Z) = \xi + \hat{\Delta}(\xi, Z)$, $ct(\xi, Z) = Z + \hat{\Xi}(\xi, Z)$. One immediately checks that $\hat{\Xi}(\xi, Z)$ is strictly increasing (hence invertible) with respect to ξ for all fixed Z , eq. (4) is solved by $\hat{\mathbf{x}}_e^\perp(\xi, Z) - \mathbf{X}^\perp = \hat{\mathbf{Y}}^\perp(\xi, Z)$, and $\hat{t}(\xi, Z)$ is the inverse of $\tilde{\xi}(t, Z) := ct - z_e(t, Z)$. Note that both

$$\hat{\mathbf{x}}_e(\xi, \mathbf{X}) = \mathbf{X} + \hat{\mathbf{Y}}(\xi, Z), \quad ct(\xi, Z) = \xi + \hat{z}_e(\xi, Z) = Z + \hat{\Xi}(\xi, Z), \quad (8)$$

can be also obtained solving for t, \mathbf{x} vs. ξ, \mathbf{X} the system of functional equations

$$\xi = ct - z, \quad \hat{\Xi}(ct - z, Z) = ct - Z, \quad \hat{\mathbf{x}} - \mathbf{X} = \hat{\mathbf{Y}}(ct - z, Z) \quad (9)$$

[the second is actually equivalent to the z -component of the third]. In general one can solve (9) in four ways for one out of $\{t, \xi\}$ and one out of $\{\mathbf{x}, \mathbf{X}\}$ as functions of the remaining two variables; thus one finds the original unknowns

$$\tilde{\xi}(t, Z) = \hat{\Xi}^{-1}(ct - Z, Z), \quad \mathbf{x}_e(t, \mathbf{X}) = \mathbf{X} + \hat{\mathbf{Y}}\left[\hat{\Xi}^{-1}(ct - Z, Z), Z\right] \quad (10)$$

and other useful relations obtained by derivations. In particular, $\partial_z \hat{z}_e \equiv 1 + \partial_z \hat{\Delta} > 0$ is a necessary and sufficient condition for the invertibility (at fixed t) of the maps $z_e : Z \mapsto z$, $\mathbf{x}_e : \mathbf{X} \mapsto \mathbf{x}$, justifying the MFD description adopted so far. By replacement we obtain the other unknowns $\mathbf{u}, \gamma, \beta, n_e$, e.g.

$$\tilde{\mathbf{u}}(t, Z) = \hat{\mathbf{u}}\left[\hat{\Xi}^{-1}(ct - Z, Z), Z\right], \quad \mathbf{u}(t, z) = \hat{\mathbf{u}}[ct - z, Z_e(t, z)], \quad (11)$$

$$n_e(t, z) = \tilde{n}_0[Z_e(t, z)] \frac{\hat{\gamma}}{\hat{s} \partial_Z \hat{z}_e} \Big|_{(\xi, Z) = (ct - z, Z_e(t, z))}. \quad (12)$$

We have thus shown that solving (5-6) (e.g. numerically) and inverting the functions $\xi \mapsto \hat{\Xi}(\xi, Z)$, $Z \mapsto z_e(t, Z)$ all unknowns can be determined explicitly.

An alternative derivation of (4-6) from the least action principle is given in [15].

Even though $\epsilon^\perp, \hat{\mathbf{u}}^\perp$ oscillate fast with ξ , since $v \geq 0$ integrating (5) makes relative oscillations of $\hat{\Delta}$ much smaller than those of v and those of \hat{s} much smaller than the former; hence, as anticipated, \hat{s} is practically smooth, see e.g. fig. 4. In vacuum ($\tilde{n}_0 \equiv 0$) it is even $\hat{s} \equiv 1$, and the equations are solved in closed form [16, 17]. Note also that the right-hand side of (5)₂ is an increasing function of $\hat{\Delta}$, because so is $\tilde{N}(Z)$. Therefore, as $v(\xi)$ is zero for $\xi \leq 0$ and positive for $\xi > 0$, then so are also $\hat{\Delta}(\xi, Z)$ and $\hat{s}(\xi, Z) - 1$. Both keep increasing until $\hat{\Delta}$ reaches a positive maximum $\hat{\Delta}(\bar{\xi}, Z)$ at the $\xi = \bar{\xi}(Z) > 0$ such that $\hat{s}^2(\bar{\xi}, Z) = 1 + v(\bar{\xi})$ ($\bar{\xi} < l$ if $v(l) = 0$), see fig. 4. The time of maximal penetration of the Z electrons is thus $\bar{t}(Z) = [Z + \hat{\Xi}(\bar{\xi}, Z)]/c$.

Eq.s (5) can be written also in the form [12] of *Hamilton equations* $q' = \partial H/\partial p$, $p' = -\partial H/\partial q$ in 1 degree of freedom: ξ , $-\hat{\Delta}$, \hat{s} play the role of t, q, p , and the Hamiltonian reads

$$\begin{aligned} H(\Delta, s, \xi; Z) &:= \gamma(s, \xi) + \mathcal{U}(\Delta; Z), \quad \gamma(s, \xi) := [s^2 + 1 + v(\xi)]/2s, \\ \mathcal{U}(\Delta; Z) &:= \frac{4\pi e^2}{mc^2} \left[\tilde{\mathcal{N}}(Z + \Delta) - \tilde{\mathcal{N}}(Z) - \tilde{\mathcal{N}}(Z)\Delta \right], \quad U(z_e; Z) := \mathcal{U}(\Delta + Z; Z), \\ \tilde{\mathcal{N}}(Z) &:= \int_0^Z dZ' \tilde{N}(Z') = \int_0^Z dZ' \tilde{n}_0(Z') (Z - Z'). \end{aligned} \quad (13)$$

Defining \mathcal{U} we have fixed the free additive constant so that $\mathcal{U}(0, Z) \equiv 0$ for each Z , $H - \sqrt{1+v}$ is positive definite.

If in particular $\tilde{n}_0(Z) = n_0\theta(Z)$ (step-shaped initial density), then by (2) the longitudinal electric force acting on the Z -electrons is

$$\hat{F}_e^z(\xi, Z) = \begin{cases} -4\pi n_0 e^2 \hat{\Delta}(\xi, Z) = \text{elastic force} & \text{if } \hat{z}_e = Z + \hat{\Delta} > 0, \\ 4\pi n_0 e^2 Z = \text{constant force} & \text{if } \hat{z}_e = Z + \hat{\Delta} \leq 0; \end{cases} \quad (14)$$

hence *as long as* $z_e \geq 0$ each Z -layer of electrons is an independent copy of the *same* relativistic harmonic oscillator, (5-6) are Z -independent and (setting $M := 4\pi n_0 e^2/mc^2$) reduce to a *single* system of two first order ODE's

$$\Delta' = \frac{1+v}{2s^2} - \frac{1}{2}, \quad s' = M\Delta, \quad (15)$$

$$\Delta(0) = 0, \quad s(0) = 1; \quad (16)$$

correspondingly, the inverse function $Z_e(t, z)$ has the closed form

$$Z_e(t, z) = ct - \Xi(ct - z) = z - \Delta(ct - z). \quad (17)$$

In fig. 4 we plot a typical pump and the corresponding solution of (15-16); for $\xi \geq l$ $v(\xi) = v(l) \equiv \text{const} \simeq 0$, the equations become autonomous, all paths in phase space become cycles around the center $C := (\Delta, s) = (0, \sqrt{1+v(l)})$, and the solutions periodic of period cT_H ; hence the final result of the pulse interaction is to move the electrons from the center to a cycle of higher energy.

2.2 Finite R corrections and experimental predictions

Since $R < \infty$ the potential energies (parametrized by $Z > 0$) $U(z_e, Z)$ associated to (2) - due to charge separation - are inaccurate as $z_e \rightarrow -\infty$. Hence we replace $U \mapsto U_R$ in the equations

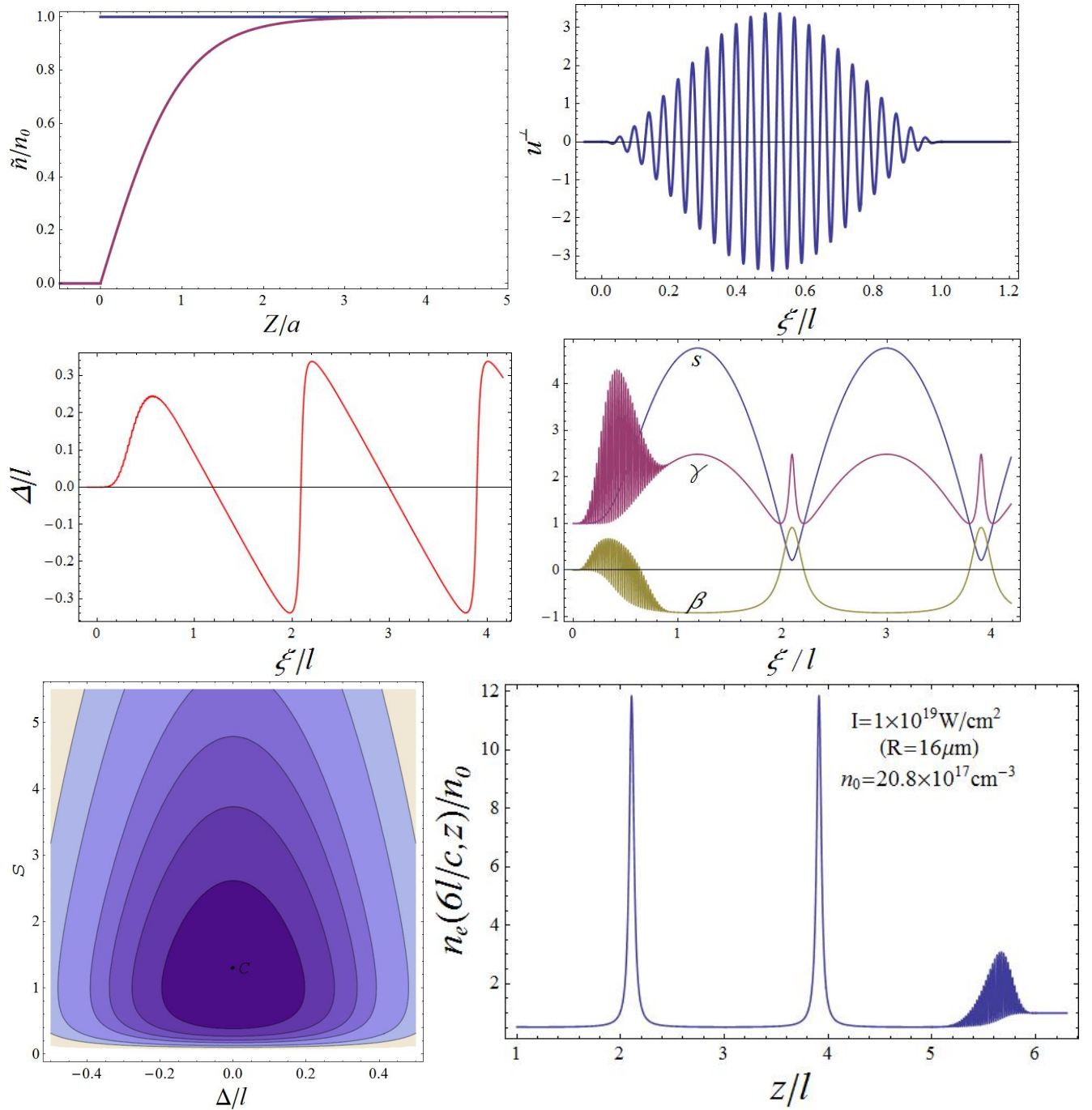


Figure 4: Up-left: the normalized \tilde{n}_0 's adopted here: step-shaped (blue) or continuous $\tilde{n}_0(Z) = n_0 \theta(Z) \tanh(Z/a)$, $a = 20 \mu\text{m}$ (purple); they respectively model the initial electron densities at the vacuum interfaces of an aerogel and of a gas jet (just outside the nozzle). Up-right: normalized pump amplitude $\hat{u}^+ \frac{10 e \alpha}{m c^2}$ of a pulse as in table 1, $R = 16 \mu\text{m}$ ($\hat{u}^+(\xi) = 0$ outside $0 < \xi < l = 18.75 \mu\text{m}$). Center: corresponding solution of (15-16) for $MI^2 = 26$ (i.e. $n_0 = 20.8 \times 10^{17} \text{ cm}^{-3}$; down-right: corresponding electron density for $z \gtrsim 20 \mu\text{m}$ about 600 fs after the impact of the laser on the plasma. Down-left: phase space paths of (15-16) with $v \equiv 0$, $MI^2 = 26$ and growing values of the total energy.

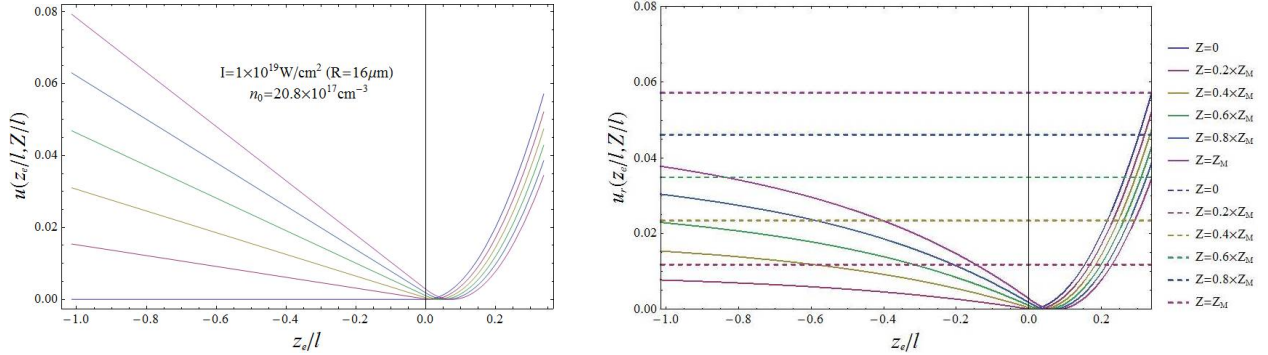


Figure 5: Rescaled longitudinal electric potential energies in the idealized plane wave (left) and in the $R=16\mu\text{m}$ (right) case, plotted as functions of z_e for $Z/Z_M = 0, .2, .4, .6, .8, 1$; the horizontal dashed lines are the left asymptotes of u_r for the same values of Z/Z_M .

of motion, where U_R is a suitable effective potential differing from U for $z_e < 0$; this allows $z_e(t, Z) \xrightarrow{t \rightarrow \infty} -\infty$ (backward escape) for electrons in a suitable surface layer $0 \leq Z \leq Z_M$. If e.g. $\tilde{n}_0(Z) = n_0\theta(Z)$ then U, U_R (plot in fig. 5) are given by $U(z_e, Z) = 2\pi n_0 e^2 [\theta(z_e) z_e^2 - 2z_e Z + Z^2]$ and

$$U_R(z_e, Z) = \pi n_0 e^2 \left[(z_e - 2Z) \sqrt{(z_e - 2Z)^2 + R^2} - 4Z z_e + R^2 \sinh^{-1} \frac{z_e - 2Z}{R} - z_e \sqrt{z_e^2 + R^2} - R^2 \sinh^{-1} \frac{z_e}{R} + 2Z^2 + 2Z \sqrt{4Z^2 + R^2} + R^2 \sinh^{-1} \frac{2Z}{R} \right].$$

Solving the equations the map $\mathbf{X} \mapsto \mathbf{x}_e(t, \mathbf{X})$ turns out to be one-to-one for all t and either sufficiently small or sufficiently large Z , showing the *self-consistency* of this MFD treatment. This was not granted by the equations alone: the invertibility of the map $\mathbf{X} \mapsto \mathbf{x}_e(t, \mathbf{X})$ fails with a large class of initial conditions [18]². For instance, in the non-relativistic limit (15) with $v \equiv 0$ is equivalent to $\hat{\Delta}'' = -M\hat{\Delta}$, which with the conditions $\hat{\Delta}(0; Z) \equiv 0$, $\hat{\Delta}'(0; Z) \equiv aZ$ is solved by

$$z_e(\xi, Z) - Z = \Delta(\xi; Z) = aZ \sin(\sqrt{M}\xi), \quad \Rightarrow \quad \frac{\partial \hat{z}_e}{\partial Z} = 1 + a \sin(\sqrt{M}\xi);$$

hence $\partial \hat{z}_e / \partial Z = 1$ at $\xi = 0$, but if $|a| > 1$ then $\partial \hat{z}_e / \partial Z < 0$ at sufficiently large ξ (or times). Sample trajectories of small Z electrons are shown in fig. 6. The interplay of the ponderomotive, electric forces yield the longitudinal forward and backward drifts at the basis of the slingshot effect. On the contrary, transverse oscillations due to \mathbf{E}^\perp average to zero

²With the initial conditions (6) and a non-vanishing v as considered here the invertibility of the map $\mathbf{X} \mapsto \mathbf{x}_e(t, \mathbf{X})$ breaks also in an intermediate Z -range ($Z_M \leq Z \leq Z'_M$) for $t \gtrsim T_H$.

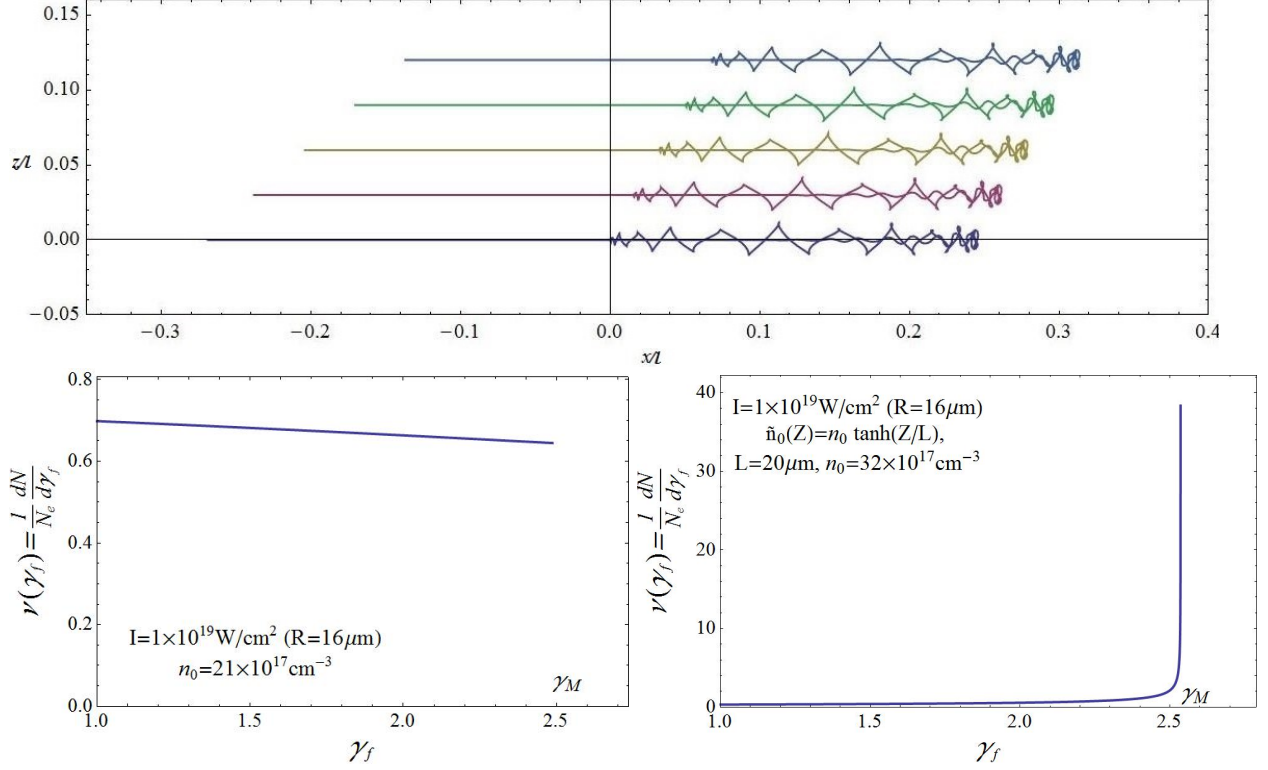


Figure 6: Up: trajectories (after 150 fs) of electrons initially located at $Z/Z_M = 0, 0.25, 0.5, 0.75, 1$ under the same conditions as in fig. 4. Down: Spectra of the expelled electrons for average pulse intensity $I = 10^{19} \text{ W/cm}^2$ and some step-shaped (left) or continuous (right) initial density \tilde{n}_0 .

and yield vanishing final transverse drift and momentum, if - as usual - the pump (1) (here polarized in the x -direction)

$$\epsilon^+(\xi) = \hat{\mathbf{x}}\epsilon_s(\xi) \cos k\xi \quad \text{with } |\epsilon'_s| \ll |k\epsilon_s| \quad (18)$$

has a slow modulation ϵ_s in the support $0 < \xi < l$; this implies $p^+(\xi) \simeq \epsilon_s(\xi) |\sin(k\xi)e/kc| = 0$ for $\xi \geq l$, and hence a good collimation of the expelled electrons. If the plasma is created by the impact on a supersonic gas jet (e.g. helium) of the pulse itself, then $l < \infty$ is the length of the interval where the intensity is sufficient to ionize the gas. The EM energy \mathcal{E} carried by a pulse (1), (18) is

$$\mathcal{E} \simeq \frac{R^2}{8} \int_0^l d\xi \epsilon_s^2(\xi). \quad (19)$$

pulse energy $\mathcal{E} \simeq 5\text{J}$, wavelength $\lambda \simeq .8\mu\text{m}$, fwhm $l' \simeq 7.5\mu\text{m}$, duration $\tau' = 25\text{fs}$							
type of target	hj	hj	hj	hj	hj	ag	ag
pulse spot radius $R (\mu\text{m})$	16	8	4	2	2	2	1
average intensity $I (10^{19} \text{ W/cm}^2)$	1	4	16	64	64	64	255
asymptotic density $n_0 (10^{19} \text{ cm}^{-3})$	0.8	2	13	80	20	12	40
maximal relativistic factor γ_M	2.6	6	8.5	14	21	12.4	22.6
maximal expulsion energy (MeV)	1.3	3	4.4	7.2	11	6.4	11.5

Table 1: Sample inputs and corresponding outputs if the target is: a supersonic helium jet (hj) or an aerogel (ag) with resp. continuous and step-shaped initial densities profiles as in fig. 4. The expelled electron charge is in all cases a few 10^{-10}C

\mathcal{E} depends on the laser; reducing R (focalization) increases the intensity I , the electron penetration ζ and the slingshot force. But we need to tune R so that U_R be justified, i.e. the “information about the finite R ” (contained in the retarded fields generated by charge separation) reach the \vec{z} -axis around the expulsion time t_e (neither much earlier, nor much later). Moreover, R must be large enough for the Forward Boosted Electrons (FBE) in an inner cylinder $\rho \leq r \leq R$ to be expelled before Lateral Electrons (LE), initially located outside the surface of the hole C_R created by the pulse and attracted towards the \vec{z} -axis, obstruct their way out. These conditions amount to [2, 19]

$$\frac{[t_e - \bar{t}]c}{R} \sim 1, \quad r := R - \frac{\zeta(t_e - l/c)}{2(t_e - \bar{t})} \theta(ct_e - l) > 0, \quad (20)$$

which can be fulfilled also with a rather small R , by the delay inherent to the retarded potential itself and the fact that contributions by ions and FBE sum up on their surface of separation, while they partially cancel on LE.

We report in table 1 and fig. 6 sample results of extensive numerical simulations performed using as inputs the parameters available in possible experiments at the FLAME facility of the Laboratori Nazionali di Frascati: a gaussian modulating intensity with full width at half maximum (fwhm) $l' \simeq 7.5\mu\text{m}$ (corresponding to a time $\tau' = 25\text{fs}$), wavelength $\lambda \simeq 0.8\mu\text{m}$, $\mathcal{E} = 5\text{J}$, R tunable in the range $1 \div 10^4 \mu\text{m}$; a supersonic helium jet or an aerogel (if $\tilde{n}_0(Z) = n_0 \theta(Z)$ with $n_0 \gtrsim 48 \times 10^{18} \text{ cm}^{-3}$) as targets. The energy spectrum, or equivalently the distribution $\nu(\gamma_f)$ of the expelled electrons vs. their final relativistic factor, depends substantially on \tilde{n}_0 , R ; pleasantly, in the case $\tilde{n}_0(Z) = n_0 \theta(Z) \tanh(Z/a)$ it is peaked (almost monochromatic) around γ_M , the maximal γ_f .

On the other hand, for Z so large that $z_e(t, Z)$ keeps positive the map $\mathbf{x}_e : \mathbf{X} \mapsto \mathbf{x}$ is

again invertible and the solution (10) can be considered reliable (by causality) for small ρ/R and for $ct - z$ bounded by few cT_H . In particular, if $\tilde{n}_0(Z) = n_0\theta(Z)$ then by (12), (17) well inside the plasma $n_e(t, z)$ is a travelling-wave with periodic peaks following the laser pulse, see fig. 4 down-right. This describes the *plasma wakefield* in the *plane wave* idealization [12]; as said, this can be considered reliable only for small ρ/R and $ct - z$ bounded by few cT_H .

Summing up, we have proposed: 1. a new laser-induced “slingshot” acceleration mechanism, which should yield well-collimated bunches of electrons of energies up to few tens MeV and is easily testable with present equipments; 2. a MFD description of the plasma wakefield just behind the laser pulse.

References

- [1] G. Fiore, R. Fedele, U. de Angelis, *The slingshot effect: a possible new laser-driven high energy acceleration mechanism for electrons*, Phys. Plasmas **21** (2014), 113105.
- [2] G. Fiore, S. De Nicola, *A simple model of the slingshot effect*, arXiv:1509.04656.
- [3] P. M. Woodward, *A method of calculating the field over a plane aperture required to produce a given polar diagram*, J. Inst. Electr. Eng., 93, 1554 (1947).
- [4] J. D. Lawson, *Lasers and accelerators*, IEEE Trans. Nucl. Sci. NS-26, 4217 (1979).
- [5] R. B. Palmer, *Laser-driven grating LINAC*, 1980, Part. Accel. 11, 81.
- [6] E. Esarey, P. Sprangle, J. Krall, *Laser acceleration of electrons in vacuum*, Phys. Rev. **E52** (1995), 5443.
- [7] T. Tajima, J. M. Dawson, *Laser Electron Accelerator*, Phys. Rev. Lett. **43**, 267270 (1979).
- [8] S.P. Mangles, et al., *Monoenergetic beams of relativistic electrons from intense laser-plasma interactions*, Nature **431** (2004), 535.
- [9] C. G. R. Geddes, et al., *High-quality electron beams from a laser wakefield accelerator using plasma-channel guiding*, Nature **431** (2004), 538.
- [10] J. Faure, et al., *A laser-plasma accelerator producing monoenergetic electron beams*, Nature **431** (2004), 541.
- [11] X. Wang, et al., *Quasi-monoenergetic laser-plasma acceleration of electrons to 2GeV*, Nat. Commun. **4** (2013), article nr.: 1988.

- [12] G. Fiore, *A plane-wave model of the impact of short laser pulses on diluted plasmas*, in preparation.
- [13] P. L. Bhatnagar, E. P. Gross, M. Krook, *A Model for Collision Processes in Gases. I. Small Amplitude Processes in Charged and Neutral One-Component Systems*, Phys. Rev. **94** (1954), 511-525.
- [14] G. Fiore , A. Maio, P. Renno, *On the initial-value problem in a cold plasma model*, Ric. Mat. **63** (2014), Suppl. 1, 157-164; and references therein.
- [15] G. Fiore, *Travelling waves and a fruitful ‘time’ reparametrization in relativistic electrodynamics*, in preparation.
- [16] G. Fiore, *On plane-wave relativistic electrodynamics in plasmas and in vacuum*, J. Phys. A: Math. Theor. **47** (2014), 225501.
- [17] G. Fiore, *On plane waves in diluted relativistic cold plasmas*, Acta Appl. Math. **132** (2014), 261-271.
- [18] J. D. Dawson, *Nonlinear electron oscillations in a cold plasma*, Phys. Rev. **113** (1959), 383.
- [19] G. Fiore, *A “slingshot” laser-driven acceleration mechanism of plasma electrons*, Nucl. Instr. Meth. Phys. Res. A, DOI: 10.1016/j.nima.2016.02.085